Dimers of Plasmonic Nanocubes to Reach Single-Molecule Strong Coupling with High Emission Yields

Jeanne Heintz,[†] Francesca Legittimo,[†,‡] and Sébastien Bidault[*,†]

†*Institut Langevin, ESPCI Paris, Université PSL, CNRS, 1 rue Jussieu, 75005 Paris, France*

‡*Current address: Dipartimento di Scienza Applicata e Tecnologia, Politecnico di Torino, Corso Duca Degli Abruzzi, 24, 10129 Torino, Italy*

E-mail: sebastien.bidault@espci.fr

Abstract

Reaching reproducible strong coupling between a quantum emitter and a plasmonic resonator at room temperature, while maintaining high emission yields, would make quantum information processing with light possible outside of cryogenic conditions. We theoretically propose to exploit the high local curvatures at the tips of plasmonic nanocubes to reach Purcell factors in excess of 10^6 at visible frequencies, rendering single-molecule strong coupling more easily accessible than with the faceted spherical nanoparticles used in recent experimental demonstrations. In the case of gold nanocube dimers, we highlight a trade-off between coupling strength and emission yield that depends on the nanocube size. Electrodynamic simulations on silver nanostructures are performed using a realistic dielectric constant, as confirmed by scattering spectroscopy performed on single nanocubes. Dimers of silver nanocubes feature similar Purcell factors than gold while allowing emission yields above 60%, thus providing design rules for efficient strongly-coupled hybrid nanostructures at room temperature.

Keywords: strong coupling, plasmonics, nanocubes, scattering spectroscopy, silver

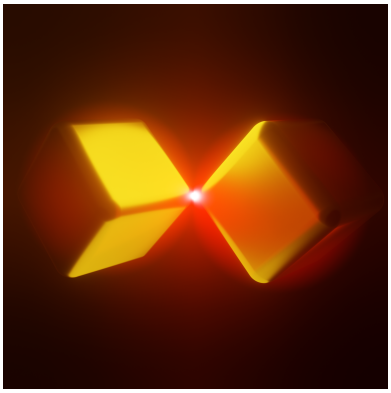

Graphical TOC Entry

Entangling light and matter by bringing quantum emitters in a strong coupling regime with a resonant cavity[1] is essential for the optical processing of quantum information, in particular by allowing few-photon nonlinearities.[2–5] While single-emitter strong coupling has been efficiently achieved with dielectric microcavities at liquid helium temperatures,[6–8] observing this phenomenon outside of a cryostat remains an open challenge.[9] Femtosecond-scale electron-phonon coupling occurring in quantum emitters at room temperature imply that they can only efficiently interact with broadband resonators, which, as a result, must confine optical fields at scales much smaller than the wavelength of light in order to maintain a large Purcell effect and thus efficient emitter-resonator coupling strengths.[9,10]

This is one of the promises of plasmonic antennas, which feature a combination of low quality factors and deep sub-wavelength mode volumes.[11,12] Recently, few-emitter strong coupling, down to a single emitter, was observed in a number of plasmonic resonators with nanoscale gaps based either on self-assembled nanostructures (nanoparticle on mirror[13–15] - NPoM - or dimer geometries)[16] or top-down fabricated antennas (on substrates[17] or on a scanning probe tip).[18] However, these phenomena were not observed in a reproducible or scalable way and the coupled systems generally feature low emission quantum yields in order to maximize the quality factor of the resonator. In particular, while scanning probe microscopy allows an active control of the emitter-resonator coupling strength, this approach is incompatible with on-chip integration.[18] For self-assembled and lithographically fabricated nanostructures, numerous issues remain: the number of emitters is not controlled *a priori*[13,17,19] or the coupling strength is below the visibility criterion for strong coupling[14] or strong coupling is only observed in a few percent of the sample.[16,19]

The influence of local facets and tips in polycrystalline gold nanoparticles (AuNPs) was recently highlighted as a possible reason for the low probability in observing strong coupling in NPoM resonators and AuNP dimers.[16,19] Indeed, the lightning-rod effect[20] favors larger field confinements and enhancements specifically if the emitter is positioned in close proximity to a tip, while the inverse effect is observed near a crystalline facet.[16] However, it is not possible

to specifically position emitters on the tips of polycrystalline nanoparticles. Alternatively, DNA-based self-assembly, in particular with the use of DNA origamis, has the ability to organize anisotropic particles with an excellent control over their relative orientation[21–23] or to functionalize their tips or facets specifically.[24] It is thus interesting to investigate whether designing plasmonic resonators in which emitters are positioned between the tips of anisotropic particles would facilitate the reproducible observation of single-molecule strong coupling at room temperature.

Anisotropic plasmonic particles, such as nanorods,[25] nanobipyramids[26] or nanocubes,[24,27] offer high local curvatures that are associated with larger field confinements and enhancements than nanospheres. Dimers of nanorods or nanobipyramids are however ill-suited to couple efficiently with fluorescent molecules that emit at visible frequencies since their resonances are redshifted to the near infrared.[28] This is not the case for plasmonic nanocubes, for which the plasmon resonance wavelengths are only slightly redshifted with respect to nanospheres.[29] Furthermore, monodisperse and monocrystalline gold nanocubes (AuNCs) with sharp tips were demonstrated in the literature[29] as well as silver nanocubes[30] (AgNCs), allowing an extra degree of freedom to optimize visible strong coupling and emission yields in the considered plasmonic resonators by exploiting the lower non-radiative decay channels in silver nanostructures.[31]

This is why we investigate here the ability of dimers of silver or gold nanocubes to reach a strong coupling regime with a single fluorescent molecule, while maintaining high emission yields. Electrodynamic simulations demonstrate that local field enhancements and Purcell factors are larger in dimers of AuNCs than in dimers of gold nanospheres (AuNSs) or of polycrystalline AuNPs, relaxing the conditions for which the visibility criterion for strong coupling can be reached when coupled to a single emitter. These calculations indicate a trade-off between emission yield and visible strong coupling in AuNC dimers, which can be tailored by tuning the size of the nanocubes. Since there is an ongoing debate in the literature on the choice of the bulk dielectric function of silver to analyze nanoparticles,[31] we

compare single AgNC scattering spectroscopy measurements to simulations performed with the most commonly used Ag dielectric functions in order to validate our model. Comparing theoretical strong coupling conditions in dimers of gold and silver nanocubes, we observe that AgNCs combine an increase in quality factor with a significant gain in emission yield. Our results therefore provide realistic plasmonic architectures in which single-molecule strong coupling can be achieved in a robust and reproducible way, while allowing photon emission yields well above 50%.

The coupling strength g between a single quantum emitter and a plasmonic resonator depends on the Purcell factor of the resonator F_p for a given position and orientation of the emitter, as well as the damping rate of the resonator γ_p and the radiative decay rate of the emitter without the resonator Γ_{R0}:[9,16,32] $g = \sqrt{F_p \gamma_p \Gamma_{R0}}/2$. F_p corresponds to the change in the local density of optical states (LDOS) for the emitter in the resonator, relative to a homogeneous medium,[32] and is computed by substituting the quantum emitter for a classical dipole and inferring its total dissipated power with the resonator P_{tot} and its total radiated power without it P_{R0}: $F_p = P_{tot}/P_{R0}$.[16,33,34] By considering that the electronic resonance of the emitter ω_0 matches the plasmonic resonance $\omega_p = \omega_0$, it is possible to define a visible strong coupling figure of merit corresponding to a coupling rate between emitter and resonator faster than the sum of all loss rates: $4g/(\gamma_p + \gamma_0) > 1$, with γ_0 the dephasing rate of the emitter.[9,14–16,35,36]

Classical electrodynamic simulations also allow an estimation of the radiative yield Φ of the coupled emitter-resonator by calculating the power radiated by the dipole P_R in the resonator: $\Phi = P_R/P_{tot}$. In the weak coupling regime, for values of F_p of several orders of magnitude, Φ is generally similar to the final emission quantum yield of the coupled system, unless the initial quantum yield of the emitter is close to 0.[34,37] Furthermore, by exciting the plasmonic resonator with a plane wave polarized along the dimer axis with a wavelength matching the longitudinal resonance, we can estimate the maximum enhancement of the electric field in the gap of the antenna.

In order to highlight the influence of high local curvatures on the emitter-resonator coupling strength, let us first consider the gain in local field enhancement, Purcell factor and strong coupling figure of merit when going from a perfect gold nanosphere to a gold nanocube at fixed nanoparticle volume. Recent experimental realizations have shown that a sharp AuNC typically features a radius of curvature at the tip corresponding to ∼10% of the nanocube edge length, compared to ∼25% for a rounded cube.[29] We thus compare in Figure 1-a the local field enhancement observed in a 2 nm gap between two 40 nm diameter AuNSs and two rounded or sharp 30 nm AuNCs (to provide similar particle volumes and with radii of curvatures of 7.5 nm and 3 nm, respectively), using Boundary Element Method (BEM)[38,39] simulations performed with tabulated data for the dielectric constant of gold[40] and an optical index of 1.4 for the environment as observed in recent strong coupling measurements in AuNP dimers.[16] These nanoparticle sizes and gap lengths were chosen as they were recently shown, theoretically and experimentally, to provide the onset of few-molecule strong coupling for spherical AuNPs.[16] BEM simulations allow the study of anisotropic plasmonic particles and are compatible with extreme nanoscale gaps, down to 1 nm.[16] Simulations are not performed with interparticle spacings below 1 nm to avoid the influence of quantum non-local effects.[41,42] However, these simulations consider a point-like source dipole and neglect the dependence of the dielectric function of the metal with respect to the wavevectors of the radiated electromagnetic field. Furthermore, going beyond the point-like emitter approximation would require a quantum-mechanical treatment of the electronic wavefunctions of the molecule.[43–47]

In Figure 1-a, we observe, in all cases, local field enhancements in excess of 10^5 in the center of the dimers, with a gain of nearly an order of magnitude for the sharp AuNCs compared to AuNSs. These strong local field enhancements are related to the radiative part of the Purcell factor by reciprocity[33] and, as shown in Figure 1-b, dimers of 40 nm AuNSs and 30 nm AuNCs feature values of F_p that exceed 10^6 for a 1 nm gap, when considering a dipolar emitter in the center of the dimer, oriented along its axis and with ω_0 matching the longi-

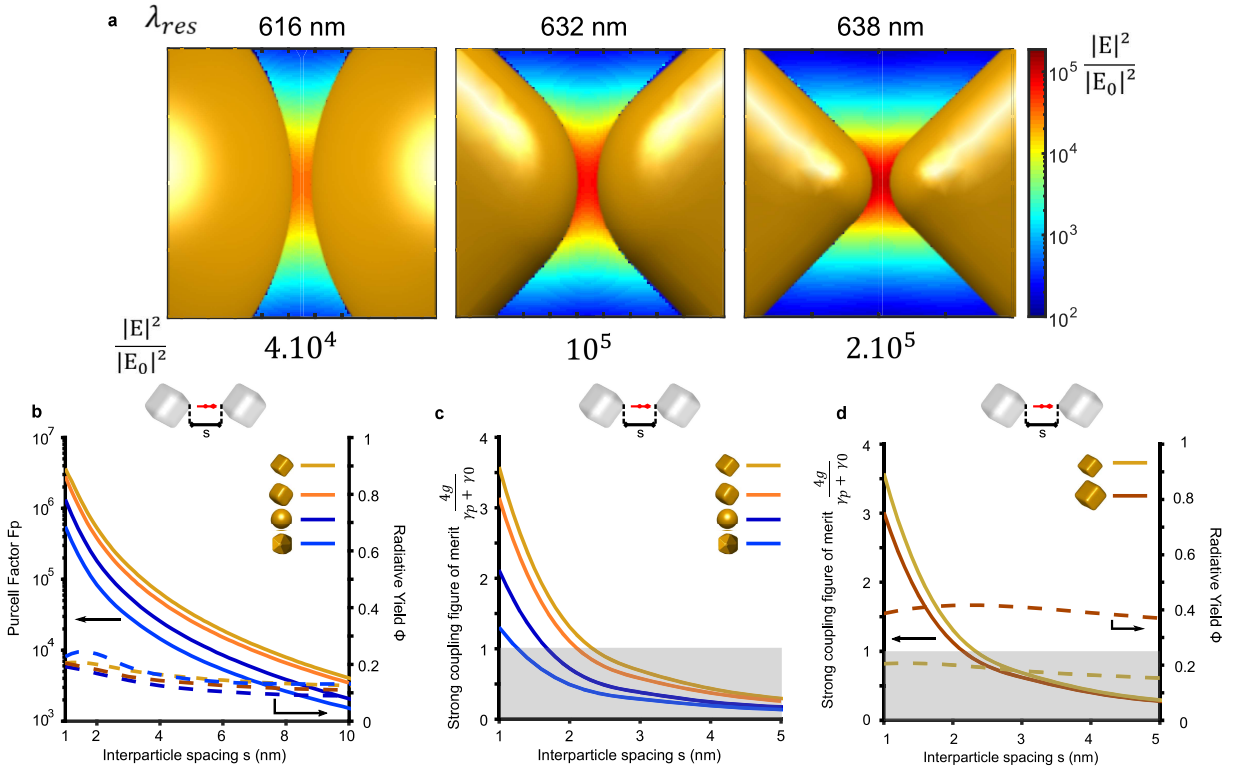

Figure 1: Increased emitter-resonator coupling in gold nanocubes. (a) Simulated local field enhancements, $|E/E_0|^2$, in the center of a dimer of 40 nm AuNSs, rounded 30 nm AuNCs or sharp 30 nm AuNCs, with a 2 nm interparticle spacing (the longitudinal resonance wavelengths and the maximum enhancements are provided on the top and bottom of the figures, respectively). (b) Computed Purcell factor F_p (solid lines), and radiative yield Φ (dashed lines), in dimers of 40 nm AuNSs (blue data), 40 nm rounded icosahedra (light blue), 30 nm rounded AuNCs (orange) and 30 nm sharp NCs (yellow) for a longitudinally coupled emitter positioned in the center and as a function of the interparticle spacing s. (c) Visible strong coupling figure of merit $4g/(\gamma_p + \gamma_0)$ (solid line, see text for details) as a function of s in the same geometry as (b). (d) Visible strong coupling figure of merit (solid lines) and Φ (dashed lines) in dimers of 30 nm (yellow) and 40 nm (red) sharp AuNCs for a longitudinally coupled emitter positioned in the center and as a function of the interparticle spacing s.

tudinal resonance of the dimer. It is important to note that while it is possible to assemble plasmonic resonators using chemically etched monocrystalline AuNSs,[48–50] recent realizations of few-molecule strong coupling were instead performed with polycrystalline faceted AuNPs, for which assembly along facets is the most probable in either NPoM or dimer geometries.[13,14,16] Since polycrystalline faceted particles are well described theoretically by rounded icosahedra,[16,51] we also plot in Figure 1-b the values of F_p for dimers of rounded

icosahedra of the same volume and oriented along parallel facets. Figure 1-b also provides the computed values of Φ for all dimer geometries, which are similar and remain below 20%. This is logical as radiative decay channels are strongly dependent on the size of the AuNPs and particles with a volume equivalent to a 40 nm diameter sphere provide low emission yields.[16,34] However, these low radiative decay rates are related to a higher resonance quality factor and, therefore, to a higher strong coupling figure of merit.[16]

Figure 1-c shows the evolution of the strong coupling figure of merit in dimers of 40 nm AuNSs, 40 nm AuNPs and 30 nm AuNCs as a function of the interparticle spacing when considering typical values of the radiative decay rate and dephasing time for the dipolar emitter ($\Gamma_{R0} = 0.2$ μeV and $\gamma_0 = 50$ meV).[16] The computed values of the damping rate of the plasmonic resonator γ_p and of the coupling strength g, as a function of the interparticle distance, and which are needed to estimate the strong coupling figure of merit, are provided in Figure S1 of the supplementary information. We observe that using nanocubes instead of spheres or polycrystalline particles relaxes the conditions in which strong coupling should be visible in AuNP dimers. In particular, comparing simulations for the polycrystalline AuNPs aligned by facets, recently used in strong coupling experiments,[13,14,16] and the proposed sharp AuNCs assembled along their tips, we observe an increase by nearly a factor of 3 of the strong coupling figure of merit and an increase by a factor of 2 of the minimum interparticle spacing at which single-molecule strong coupling could be observed. It is important to stress that an increase of 3 for the figure of merit corresponds to an increase of g similar to what would be observed when coupling 9 emitters identically with a given plasmonic resonator.[13,16] Such an increase is therefore essential to go from few-molecule to single-molecule realizations of strong coupling.

While dimers of AuNCs would provide a significant gain in Purcell factor and coupling strength compared to similarly sized spherical AuNPs, Figure 1-b indicates a negligible gain in emission yield. To investigate whether increasing the size of the nanocubes could provide larger values of Φ without sacrificing the coupling strength, we compare in Figure 1-d the

evolution of the figure of merit and of the emission yield as a function of the particle spacing for dimers of sharp 30 nm and 40 nm AuNCs (with radii of curvature of 3 nm and 4 nm, respectively). These simulations indicate that the faster resonator decay rate γ_p, associated with larger particles, increases Φ by a factor of 2 and lowers the strong coupling figure of merit by a modest 20%. This means that, by tuning the nanoparticle size, it is possible to favor either the coupling strength or the emission yield and that dimers of AuNCs could be strongly coupled to a single molecule while maintaining a final emission yield close to 50%. To further increase Φ while maintaining visible strong coupling, one solution is to decrease the non-radiative decay rate in the resonator, for instance by substituting gold for silver. This is another reason why nanocubes are attractive as high quality AgNCs were experimentally demonstrated[30] and can be exploited in self-assembled nanostructures using DNA nanotechnology.[52] However, there was a recent debate on the choice of the dielectric function of silver that provides the best agreement with single particle spectroscopy.[31] Indeed, when studying the dipolar mode of single spheres, the two most widely used dielectric functions reported by Johnson and Christy[40] or by Palik[53] both provide good agreements with simulations performed using slightly different nanoparticle sizes.[31] However, the ohmic losses in the Palik data set are significantly larger in the visible range than for Johnson and Christy, providing very different strong coupling figures of merit. On the other hand, more recent measurements performed on silver films indicate similar values of the real part of the dielectric function compared to Johnson and Christy but a slightly larger imaginary part.[54]

To investigate which dielectric function provides the best agreement with the optical properties of silver nanocubes, we study 78 nm AgNCs, with an estimated radius of curvature of 9 nm (estimated from electron microscopy images, see Figure 2-a), using both ensemble extinction measurements in ethanol (Figure 2-b) and single particle scattering spectroscopy on particles spin-coated on a glass coverslip and covered in index-matching oil to minimize the oxidation of silver (typical examples in Figures 2-c-d). The scattering spectra of single AgNCs are simulated in BEM using the three reported dielectric constants of silver and a

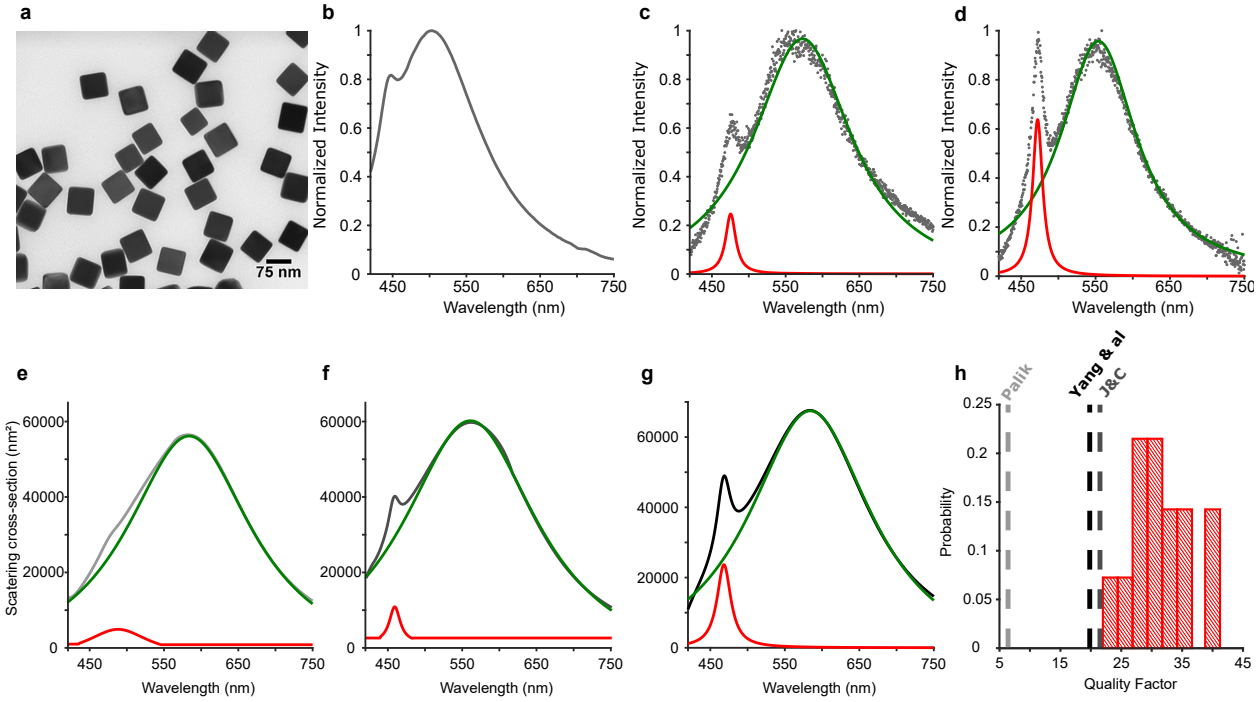

Figure 2: Comparison between experiments and simulations on single silver nanocubes. (a) Typical electron microscopy image of 78 nm AgNCs with an estimated radius of curvature of 9 nm. (b) Ensemble extinction spectrum of 78 nm AgNCs in ethanol. (c-d) Typical single AgNC scattering spectra. Simulated scattering spectra of 78 nm AgNCs using the dielectric constant of Palik[53] (e), Johnson and Christy[40] (f) and Yang et *al*. (g).[54] Experimental and simulated scattering sepctra in (c-g) are fitted by two energy-dependent Lorentzian functions (green and red solid lines). (h) Distribution of quadrupolar quality factors measured with 14 single AgNCs, compared to the theoretical values inferred from the simulations in (e-g).

1.5 surrounding refractive index (Figures 2-e-g).

The ensemble spectrum in Figure 2-b clearly shows two resonances with a broad dipolar mode around 515 nm and a narrow blue-shifted quadrupolar mode. These two modes are also visible in the scattering spectra of single AgNC but are red-shifted due to the larger refractive index of index matching oil compared to ethanol. The simulated spectra show similar behaviors for the dipolar mode but radically different responses for the quadrupolar resonance. Indeed, the dipolar mode, which is dominated by radiative damping, features a similar resonance wavelength and quality factor in the measurements and in the simulations, but the quality factor of the quadrupolar mode, which is dominated by non-radiative losses,

is strongly underestimated using the dielectric constant reported by Palik. A more quantitative analysis of this difference can be observed in Figure 2-h with a comparison of the quality factors of the quadrupolar modes inferred from the simulations and experimentally estimated for 14 single AgNCs. The quality factors are estimated by fitting the simulated and experimental spectra using an energy-dependent double Lorentzian function.

The data on Figure 2-h evidence that the Johnson and Christy dielectric constant provides the best agreement with experimental data. Interestingly, all measured quality factors are larger than the simulated ones. This indicates that even the Johnson and Christy data might overestimate the imaginary part of the dielectric constant of silver in colloidal nanocubes, even though more recent measurements on silver films typically feature similar or slightly larger values.[54] This may be due to a thin silver oxide layer influencing the measurements performed on silver films in contact with air, compared to silver nanoparticles in water or protected by index matching oil. For instance, similar scattering spectral measurements performed on deposited single AgNCs in contact with air do not feature sharp quadrupolar modes. Overall, this comparison between experiments and theory means that BEM simulations on dimers of AgNCs provide conservative values of the expected strong coupling figure of merit.

Figure 3-a shows the computed Purcell factors and emission yields in the center of 30 nm AgNC dimers (with a 3 nm radius of curvature) compared to the values obtained with 30 nm and 40 nm AuNCs. We observe that the values of F_p for silver and gold nanocubes are nearly identical, indicating that the local curvature is probably the main parameter in optimizing the confinement and enhancement of the local electric field. However, since AgNCs feature lower ohmic losses, the emission yield is nearly 2 times larger for silver and the strong coupling figure of merit in Figure 3-b is 10% larger than for gold (values of γ_p and g for these dimer geometries are provided in Figure S1). Interestingly, the simulated values of γ_p in Figure S1 indicate that the damping rate of the resonator should reach values of the order of 100-150 meV for interparticle gaps compatible with strong coupling for both

AuNC and AgNC dimers. If we consider that the total decay rate of the molecule by itself Γ_0 is negligible compared to γ_p (unless the initial quantum yield is nearly 0) and that the two strongly-coupled eigenmodes equally share the damping rates of the emitter and of the resonator behaving as damped harmonic oscillators (as expected in the Jaynes-Cummings model),[16,32] this means that the final decay times of the strongly-coupled eigenmodes should be of the order of 10 fs and thus slightly lower than the considered dephasing time $\hbar/\gamma_0$ =12 fs of the isolated molecule (with $\hbar$ the reduced Planck constant).

Furthermore, if the resonator dominates both the radiative and non-radiative damping rates of the coupled system, then both eigenmodes should feature emission yields equal to Φ. These results thus indicate how dimers of 30 nm silver nanocubes should allow single-molecule strong coupling at room temperature with an emission yield well above 50%. A potential limiting factor for AgNC dimers that is not considered in these simulations is the possible appearance of a thin silver oxide layer on the surface of the nanocubes, which would effectively increase the interparticle distance. However, the sharp quadrupolar modes observed experimentally on single AgNCs in Figure 2 indicate that this effect should be limited if the particles are kept from direct contact with air. For long-term stability of these hybrid nanostructures, AuNC dimers, with only slightly lower coupling strengths and emission yields, are an appealing alternative.

We can also observe in Figure 3-a that the distance dependence of Φ is different for the considered AuNC and AgNC dimers. This is due to the wavelength dependence of the imaginary part of the dielectric constants of gold and silver and to the dependence of the longitudinal resonance of dimers with respect to interparticle spacings. In these simulations, we consider that the resonance of the emitter matches the longitudinal resonance wavelength of the plasmonic dimer ω_p. Since the minimum imaginary part of the dielectric function of gold is around 680 nm,[55] the maximum emission yield will typically be observed when ω_p reaches this wavelength, which occurs for an interparticle spacing around 2 nm for 40 nm AuNCs, compared to $\sim$1 nm for 30 nm gold cubes. In the case of silver, the imaginary part of the

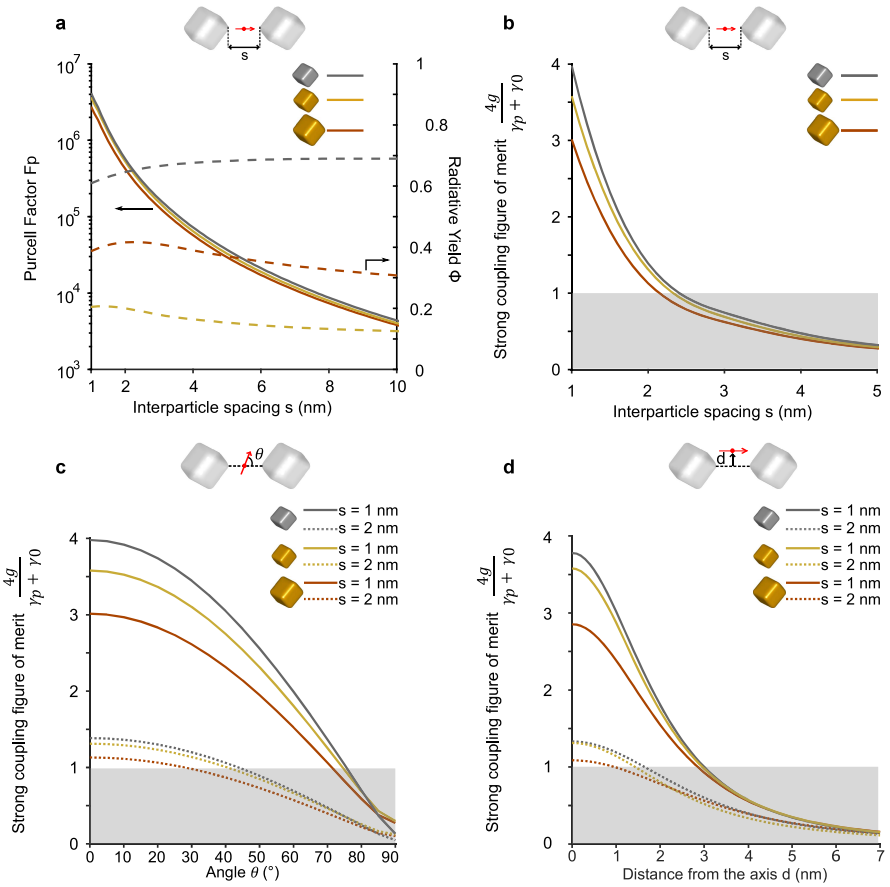

Figure 3: Strong coupling with high emission yields in dimers of silver nanocubes. (a) Computed Purcell factor F_p (solid lines), and radiative yield Φ (dashed lines), in dimers of 30 nm AgNCs (grey data), 30 nm AuNCs (yellow) and 40 nm AuNCs (red) for a longitudinally coupled emitter positioned in the center and as a function of the interparticle spacing s. (b) Visible strong coupling figure of merit (solid line) as a function of s in the same geometry as (a). (c) Visible strong coupling figure of merit as a function of the orientation of the dipolar emitter in dimers of 30 nm AgNCs (grey data), 30 nm AuNCs (yellow) and 40 nm AuNCs (red) with 1 nm (solid solid line) and 2 nm (dotted line) spacings. (d) Visible strong coupling figure of merit for a longitudinal emitter as a function of its position with respect to the dimer axis, for dimers of 30 nm AgNCs (grey data), 30 nm AuNCs (yellow) and 40 nm AuNCs (red) with 1 nm (solid solid line) and 2 nm (dotted line) spacings.

dielectric function increases with the wavelength (as can be expected for a Drude metal),[54] explaining the decrease of Φ when the particles get closer and the longitudinal resonance redshifts.

All the simulations presented in Figures 1 and 3-a-b consider a perfectly centered emitting dipole with an orientation along the dimer axis. While recent self-assembly strategies, in

particular using DNA, have shown an excellent position[10,56] and orientation[57,58] control over fluorescent molecules, it is interesting to consider how robust the appearance of a strong coupling regime will be for an imperfectly centered or oriented transition dipole. Figures 3-c-d show how the strong coupling figure of merit varies as a function of the off-axis orientation and position of the source dipole, with interparticle spacings of 1 nm and 2 nm. We observe that strong coupling should remain visible for emitters with an off-axis orientation up to 45° with a 2 nm spacing and up to 75° with 1 nm. As observed in the local field distribution of Figure 1-a, the enhancement process is maximum at the very center of the dimer as confirmed by Figure 1-d since strong coupling will only be visible if the emitter is within 2 nm or 3 nm of the dimer axis, if the interparticle spacing is 2 nm or 1 nm, respectively. While these calculations show how precise the self-assembly strategy will need to be in order to position a single emitter between the tips of two plasmonic nanocubes, it is important to stress that the tips of gold nanocubes were recently functionalized specifically with DNA strands.[24] Alternatively, one could consider a NPoM resonator geometry by assembling a plasmonic nanocube on a metallic mirror by one of its tips in order to avoid issues regarding the relative orientation of the two cubes in self-assembled dimers, while retaining a high local field enhancement and confinement. In both cases, an additional electric field enhancement could arise from the spontaneous appearance of atomic protrusions in the nanoscale gap.[59] In order to reach single-molecule strong coupling at room temperature with high emission yields, we therefore propose to exploit the high local curvatures offered by dimers of plasmonic nanocubes aligned along their tips, which feature higher coupling strengths than dimers of perfect or faceted gold nanospheres while maintaining resonance wavelengths in the visible range. Electrodynamic simulations indicate that the stringent experimental conditions at which visible strong coupling can be achieved at room temperature are significantly relaxed by the use of both AuNCs and AgNCs. It is possible to favor the coupling strength or the emission yield by tuning the nanocube size but the use of 40 nm AuNCs and 30 nm AgNCs should provide both single-molecule strong coupling and emission yields of nearly 50% for

gold and above 60% for silver. Experimental realizations with AgNCs could even exceed these expectations as the ohmic losses, experimentally observed by scattering spectroscopy on single cubes, appear lower than those theoretically expected using typical dielectric constants for silver.

Interestingly, both gold[24] and silver[52] nanocubes are compatible with DNA-based self-assembly, which has been shown as an efficient bottom-up strategy to reach strong coupling at room temperature[14,16] and which also allows a control over the orientation of dye molecules.[57,58] DNA nanotechnology thus provides all the required ingredients to produce bright strongly coupled hybrid nanostructures featuring few-photon nonlinearities at room temperature.

Methods

Simulations

Boundary Element Method simulations are performed using the MNPBEM toolbox.[39] The 2D meshing of the spheres and nanocubes are generated in Matlab while, for rounded icosahedra, the 3D meshing is first generated using COMSOL. The trapezoidal mesh for spheres is generated by longitudes and latitudes with a minimum size of 0.5 nm at the interparticle gap. The triangular mesh of nanocubes is generated as an extruded rounded polygon using dedicated functions of the MNPBEM toolbox as detailed elsewhere[39] and with a minimum mesh size of 0.2 nm at the tips. The total dissipated and radiated powers of a classical electric dipole in the resonator are compared to the power radiated without the resonator in order to compute F_p and Φ for a given position, orientation and emission wavelength. By tuning the emission wavelength for a longitudinally coupled emitter and monitoring the frequency at which the maximum total decay rate is achieved, as well as the full-width at half maximum, it is possible to infer the resonance wavelength ω_p and decay rate γ_p of the longitudinal mode of the dimer. The local field enhancements are generated by exciting the

plasmonic resonators with a plane wave polarized along the dimer axis at the longitudinal resonance wavelength. Scattering cross-sections of single silver nanocubes are computed by exciting the AgNC with a wavelength-tunable plane wave propagating perpendicularly to one face of the cube and polarized along one edge and then integrating the radiated power on a sphere around the particle.

Convergence of these simulations with respect to the mesh size was verified in the case of spheres by comparing them to Mie theory calculations and observing differences below 5% at a 1 nm interparticle gap distance and below 1% for a 2 nm gap.[16] In a general way, the data of Figure 3-d allow the observation of digital artefacts due to the mesh size when monitoring the evolution of the strong coupling figure of merit with respect to the transverse position of the source dipole. The comparison between Mie theory and BEM simulations in the case of spheres shows that a smooth and not a stepwise evolution of the strong coupling figure of merit indicates numerical convergence.

Optical Measurements

The extinction spectrum of commercial silver nanocubes (Nanocomposix, USA, 78 nm edge lengths) is measured with a typical concentration of 1 mg/mL in ethanol (Duetta, Horiba). Single AgNCs are studied in scattering spectroscopy by spin-coating 100 μL of the nanocube solution on a freshly cleaned glass coverslip and adding a few drops of index matching oil. Darkfield spectra are measured in an inverted microscope (IX71, Olympus) coupled to a fiber-coupled (50 μm core diameter) imaging spectrometer (Acton SP300 with Pixis 100 CCD detector, Princeton Instruments). White light from a 100 W halogen lamp is focused on the sample using an oil-immersion 1.2-1.4 NA dark-field condenser. Scattered light is collected with a 100 $\times$ 0.6 NA immersion oil objective. A Single AgNC is aligned with the optical fiber using a piezoelectric stage (P-562.3CD, PI) before its raw scattering spectrum is measured with a 2 s acquisition time. A background spectrum is measured with the same acquisition time on an empty area of the sample. The background is subtracted to

the measured spectra before the obtained data are divided by a smoothed background spectrum (after substracting a constant offset of the CCD detector) in order to account for the wavelength-dependent illumination and detection.[16] The extinction spectrum of commercial silver nanocubes (Nanocomposix, USA, 78 nm edge lengths) is measured with a typical concentration of 1 mg/mL in ethanol (Duetta, Horiba). Single AgNCs are studied in scattering spectroscopy by spin-coating 100 μL of the nanocube solution on a freshly cleaned glass coverslip and adding a few drops of index matching oil. Darkfield spectra are measured in an inverted microscope (IX71, Olympus) coupled to a fiber-coupled (50 μm core diameter) imaging spectrometer (Acton SP300 with Pixis 100 CCD detector, Princeton Instruments). White light from a 100 W halogen lamp is focused on the sample using an oil-immersion 1.2-1.4 NA dark-field condenser. Scattered light is collected with a 100 $\times$ 0.6 NA immersion oil objective. A Single AgNC is aligned with the optical fiber using a piezoelectric stage (P-562.3CD, PI) before its raw scattering spectrum is measured with a 2 s acquisition time. A background spectrum is measured with the same acquisition time on an empty area of the sample. The background is subtracted to the measured spectra before the obtained data are divided by a smoothed background spectrum (after substracting a constant offset of the CCD detector) in order to account for the wavelength-dependent illumination and detection.[16]

Acknowledgement

This work was supported by Agence Nationale de la Recherche via projects ANR-15-CE09-0003 and ANR-21-CE09-0010, and by LABEX WIFI (Laboratory of Excellence within the French Program "Investments for the Future") under references ANR-10-LABX-24 and ANR-10-IDEX-0001-02 PSL*.

Supporting Information Available

The Supporting Information is available free of charge on the ACS Publications website. Complementary figure providing the computed values of the damping rate of the plasmonic resonators and of the coupling strength g.

References

(1) Raimond, J. M.; Brune, M.; Haroche, S. Manipulating quantum entanglement with atoms and photons in a cavity. *Rev. Mod. Phys.* **2001**, *73*, 565–582.

(2) Birnbaum, K. M.; Boca, A.; Miller, R.; Boozer, A. D.; Northup, T. E.; Kimble, H. J. Photon Blockade in an Optical Cavity with One Trapped Atom. *Nature* **2005**, *436*, 87–90.

(3) Loo, V.; Arnold, C.; Gazzano, O.; Lemaître, A.; Sagnes, I.; Krebs, O.; Voisin, P.; Senellart, P.; Lanco, L. Optical Nonlinearity for Few-Photon Pulses on a Quantum Dot-Pillar Cavity Device. *Phys. Rev. Lett.* **2012**, *109*, 166806.

(4) Volz, T.; Reinhard, A.; Winger, M.; Badolato, A.; Hennessy, K. J.; Hu, E. L.; Imamoğlu, A. Ultrafast All-Optical Switching by Single Photons. *Nat. Photon.* **2012**, *6*, 605–609.

(5) Wang, D.; Kelkar, H.; Martin-Cano, D.; Rattenbacher, D.; Shkarin, A.; Utikal, T.; Götzinger, S.; Sandoghdar, V. Turning a molecule into a coherent two-level quantum system. *Nat. Phys.* **2019**, *15*, 483–489.

(6) Reithmaier, J. P.; Sek, G.; Löffler, A.; Hofmann, C.; Kuhn, S.; Reitzenstein, S.; Keldysh, L. V.; Kulakovskii, V. D.; Reinecke, T. L.; Forchel, A. Strong coupling in a single quantum dot–semiconductor microcavity system. *Nature* **2004**, *432*, 197–200.

(7) Yoshie, T.; Scherer, A.; Hendrickson, J.; Khitrova, G.; Gibbs, H. M.; Rupper, G.; Ell, C.; Shchekin, O. B.; Deppe, D. G. Vacuum Rabi Splitting with a Single Quantum Dot in a Photonic Crystal Nanocavity. *Nature* **2004**, *432*, 200–203.

(8) Peter, E.; Senellart, P.; Martrou, D.; Lemaitre, A.; Hours, J.; Gerard, J. M.; Bloch, J. Exciton-photon strong-coupling regime for a single quantum dot embedded in a microcavity. *Phys. Rev. Lett.* **2005**, *95*, 067401.

(9) Palstra, I. M.; Doeleman, H. M.; Koenderink, A. F. Hybrid cavity-antenna systems for quantum optics outside the cryostat? *Nanophotonics* **2019**, *8*, 1513–1531.

(10) Busson, M. P.; Rolly, B.; Stout, B.; Bonod, N.; Bidault, S. Accelerated Single Photon Emission from Dye Molecule-Driven Nanoantennas Assembled on DNA. *Nat. Commun.* **2012**, *3*, 962.

(11) Koenderink, A. F. On the use of Purcell factors for plasmon antennas. *Opt. Lett.* **2010**, *35*, 4208–4210.

(12) Sauvan, C.; Hugonin, J. P.; Maksymov, I. S.; Lalanne, P. Theory of the Spontaneous Optical Emission of Nanosize Photonic and Plasmon Resonators. *Phys. Rev. Lett.* **2013**, *110*, 237401.

(13) Chikkaraddy, R.; Nijs, B. d.; Benz, F.; Barrow, S. J.; Scherman, O. A.; Rosta, E.; Demetriadou, A.; Fox, P.; Hess, O.; Baumberg, J. J. Single-Molecule Strong Coupling at Room Temperature in Plasmonic Nanocavities. *Nature* **2016**, *535*, 127–130.

(14) Chikkaraddy, R.; Turek, V.; Kongsuwan, N.; Benz, F.; Carnegie, C.; van de Goor, T.; de Nijs, B.; Demetriadou, A.; Hess, O.; Keyser, U. F.; Baumberg, J. J. Mapping Nanoscale Hotspots with Single-Molecule Emitters Assembled into Plasmonic Nanocavities Using DNA Origami. *Nano Lett.* **2018**, *18*, 405–411.

(15) Pelton, M.; Storm, S. D.; Leng, H. Strong Coupling of Emitters to Single Plasmonic Nanoparticles: Exciton-Induced Transparency and Rabi Splitting. *Nanoscale* **2019**, *11*, 14540–14552.

(16) Heintz, J.; Markešević, N.; Gayet, E. Y.; Bonod, N.; Bidault, S. Few-Molecule Strong Coupling with Dimers of Plasmonic Nanoparticles Assembled on DNA. *ACS Nano* **2021**, *15*, 14732–14743.

(17) Santhosh, K.; Bitton, O.; Chuntonov, L.; Haran, G. Vacuum Rabi Splitting in a Plasmonic Cavity at the Single Quantum Emitter Limit. *Nat. Commun.* **2016**, *7*, 11823.

(18) Groß, H.; Hamm, J. M.; Tufarelli, T.; Hess, O.; Hecht, B. Near-Field Strong Coupling of Single Quantum Dots. *Sci. Adv.* **2018**, *4*, eaar4906.

(19) Leng, H.; Szychowski, B.; Daniel, M.-C.; Pelton, M. Strong Coupling and Induced Transparency at Room Temperature with Single Quantum Dots and Gap Plasmons. *Nat. Commun.* **2018**, *9*, 4012.

(20) Novotny, L.; Bian, R. X.; Xie, X. S. Theory of Nanometric Optical Tweezers. *Phys. Rev. Lett.* **1997**, *79*, 645–648.

(21) Kuzyk, A.; Schreiber, R.; Zhang, H.; Govorov, A. O.; Liedl, T.; Liu, N. Reconfigurable 3D Plasmonic Metamolecules. *Nat. Mater.* **2014**, *13*, 862–866.

(22) Zhan, P.; Dutta, P. K.; Wang, P.; Song, G.; Dai, M.; Zhao, S.-X.; Wang, Z.-G.; Yin, P.; Zhang, W.; Ding, B.; Ke, Y. Reconfigurable Three-Dimensional Gold Nanorod Plasmonic Nanostructures Organized on DNA Origami Tripod. *ACS Nano* **2017**, *11*, 1172–1179.

(23) Lan, X.; Su, Z.; Zhou, Y.; Meyer, T.; Ke, Y.; Wang, Q.; Chiu, W.; Liu, N.; Zou, S.; Yan, H.; Liu, Y. Programmable Supra-Assembly of a DNA Surface Adapter for Tunable

Chiral Directional Self-Assembly of Gold Nanorods. *Angew. Chem. Int. Ed.* **2017**, *56*, 14632–14636.

(24) Niu, R.; Song, C.; Gao, F.; Fang, W.; Jiang, X.; Ren, S.; Zhu, D.; Su, S.; Chao, J.; Chen, S.; Fan, C.; Wang, L. DNA Origami-Based Nanoprinting for the Assembly of Plasmonic Nanostructures with Single-Molecule Surface-Enhanced Raman Scattering. *Angew. Chem. Int. Ed.* **2021**, *60*, 11695–11701.

(25) Khatua, S.; Paulo, P. M. R.; Yuan, H.; Gupta, A.; Zijlstra, P.; Orrit, M. Resonant Plasmonic Enhancement of Single-Molecule Fluorescence by Individual Gold Nanorods. *ACS Nano* **2014**, *8*, 4440–4449.

(26) Lombardi, A.; Loumaigne, M.; Crut, A.; Maioli, P.; Del Fatti, N.; Vallée, F.; Spuch-Calvar, M.; Burgin, J.; Majimel, J.; Tréguer-Delapierre, M. Surface Plasmon Resonance Properties of Single Elongated Nano-objects: Gold Nanobipyramids and Nanorods. *Langmuir* **2012**, *28*, 9027–9033.

(27) Ge, D.; Marguet, S.; Issa, A.; Jradi, S.; Nguyen, T. H.; Nahra, M.; Béal, J.; Deturche, R.; Chen, H.; Blaize, S.; et al., Hybrid Plasmonic Nano-Emitters with Controlled Single Quantum Emitter Positioning on the Local Excitation Field. *Nat. Commun.* **2020**, *11*, 3414.

(28) Rogobete, L.; Kaminski, F.; Agio, M.; Sandoghdar, V. Design of Plasmonic Nanoantennae for Enhancing Spontaneous Emission. *Opt. Lett.* **2007**, *32*, 1623–1625.

(29) Park, J.-E.; Lee, Y.; Nam, J.-M. Precisely Shaped, Uniformly Formed Gold Nanocubes with Ultrahigh Reproducibility in Single-Particle Scattering and Surface-Enhanced Raman Scattering. *Nano Lett.* **2018**, *18*, 6475–6482.

(30) Zhou, S.; Li, J.; Gilroy, K. D.; Tao, J.; Zhu, C.; Yang, X.; Sun, X.; Xia, Y. Facile Synthesis of Silver Nanocubes with Sharp Corners and Edges in an Aqueous Solution. *ACS Nano* **2016**, *10*, 9861–9870.

(31) Baida, H.; Billaud, P.; Marhaba, S.; Christofilos, D.; Cottancin, E.; Crut, A.; Lermé, J.; Maioli, P.; Pellarin, M.; Broyer, M.; et al., Quantitative Determination of the Size Dependence of Surface Plasmon Resonance Damping in Single Ag@SiO2 Nanoparticles. *Nano Lett.* **2009**, *9*, 3463–3469.

(32) Bouchet, D.; Carminati, R. Quantum Dipole Emitters in Structured Environments: a Scattering Approach: Tutorial. *J. Opt. Soc. Am. A* **2019**, *36*, 186–195.

(33) Bharadwaj, P.; Novotny, L. Spectral Dependence of Single Molecule Fluorescence Enhancement. *Opt. Express* **2007**, *15*, 14266–14274.

(34) Bidault, S.; Devilez, A.; Maillard, V.; Lermusiaux, L.; Guigner, J.-M.; Bonod, N.; Wenger, J. Picosecond Lifetimes with High Quantum Yields from Single-Photon-Emitting Colloidal Nanostructures at Room Temperature. *ACS Nano* **2016**, *10*, 4806–4815.

(35) Törmä, P.; Barnes, W. L. Strong Coupling between Surface Plasmon Polaritons and Emitters: A Review. *Rep. Prog. Phys.* **2014**, *78*, 013901.

(36) Zengin, G.; Wersäll, M.; Nilsson, S.; Antosiewicz, T. J.; Käll, M.; Shegai, T. Realizing Strong Light-Matter Interactions between Single-Nanoparticle Plasmons and Molecular Excitons at Ambient Conditions. *Phys. Rev. Lett.* **2015**, *114*, 157401.

(37) Busson, M. P.; Rolly, B.; Stout, B.; Bonod, N.; Wenger, J.; Bidault, S. Photonic Engineering of Hybrid Metal–Organic Chromophores. *Angew. Chem. Int. Ed.* **2012**, *51*, 11083–11087.

(38) García de Abajo, F. J.; Howie, A. Retarded field calculation of electron energy loss in inhomogeneous dielectrics. *Phys. Rev. B* **2002**, *65*, 115418.

(39) Hohenester, U.; Trügler, A. MNPBEM – A Matlab Toolbox for the Simulation of Plasmonic Nanoparticles. *Comput. Phys. Commun.* **2012**, *183*, 370–381.

(40) Johnson, P. B.; Christy, R. W. Optical Constants of the Noble Metals. *Phys. Rev. B* **1972**, *6*, 4370–4379.

(41) Savage, K. J.; Hawkeye, M. M.; Esteban, R.; Borisov, A. G.; Aizpurua, J.; Baumberg, J. J. Revealing the Quantum Regime in Tunnelling Plasmonics. *Nature* **2012**, *491*, 574–577.

(42) Cha, H.; Yoon, J. H.; Yoon, S. Probing Quantum Plasmon Coupling Using Gold Nanoparticle Dimers with Tunable Interparticle Distances Down to the Subnanometer Range. *ACS Nano* **2014**, *8*, 8554–8563.

(43) Vukovic, S.; Corni, S.; Mennucci, B. Fluorescence Enhancement of Chromophores Close to Metal Nanoparticles. Optimal Setup Revealed by the Polarizable Continuum Model. *J. Phys. Chem. C* **2009**, *113*, 121–133.

(44) Sakko, A.; Rossi, T. P.; Nieminen, R. M. Dynamical coupling of plasmons and molecular excitations by hybrid quantum/classical calculations: time-domain approach. *J. Condens. Matter Phys.* **2014**, *26*, 315013.

(45) Neuman, T.; Esteban, R.; Casanova, D.; García-Vidal, F. J.; Aizpurua, J. Coupling of Molecular Emitters and Plasmonic Cavities beyond the Point-Dipole Approximation. *Nano Lett.* **2018**, *18*, 2358–2364.

(46) Doppagne, B.; Neuman, T.; Soria-Martinez, R.; López, L. E. P.; Bulou, H.; Romeo, M.; Berciaud, S.; Scheurer, F.; Aizpurua, J.; Schull, G. Single-molecule tautomerization tracking through space- and time-resolved fluorescence spectroscopy. *Nat. Nanotechnol.* **2020**, *15*, 207–211.

(47) Fregoni, J.; Haugland, T. S.; Pipolo, S.; Giovannini, T.; Koch, H.; Corni, S. Strong Coupling between Localized Surface Plasmons and Molecules by Coupled Cluster Theory. *Nano Lett.* **2021**, *21*, 6664–6670.

(48) Huh, J.-H.; Lee, J.; Lee, S. Comparative Study of Plasmonic Resonances between the Roundest and Randomly Faceted Au Nanoparticles-on-Mirror Cavities. *ACS Photonics* **2018**, *5*, 413–421.

(49) Yoon, J. H.; Selbach, F.; Langolf, L.; Schlücker, S. Ideal Dimers of Gold Nanospheres for Precision Plasmonics: Synthesis and Characterization at the Single-Particle Level for Identification of Higher Order Modes. *Small* **2018**, *14*, 1702754.

(50) Nicoli, F.; Zhang, T.; Hübner, K.; Jin, B.; Selbach, F.; Acuna, G.; Argyropoulos, C.; Liedl, T.; Pilo-Pais, M. DNA-Mediated Self-Assembly of Plasmonic Antennas with a Single Quantum Dot in the Hot Spot. *Small* **2019**, *15*, 1804418.

(51) Yoon, J. H.; Selbach, F.; Schumacher, L.; Jose, J.; Schlücker, S. Surface Plasmon Coupling in Dimers of Gold Nanoparticles: Experiment and Theory for Ideal (Spherical) and Nonideal (Faceted) Building Blocks. *ACS Photonics* **2019**, *6*, 642–648.

(52) Lermusiaux, L.; Nisar, A.; Funston, A. M. Flexible Synthesis of High-Purity Plasmonic Assemblies. *Nano Res.* **2021**, *14*, 635–645.

(53) Palik, E. D., Ed. *Handbook of Optical Constants of Solids*; Academic Press: New York, 1985.

(54) Yang, H. U.; D'Archangel, J.; Sundheimer, M. L.; Tucker, E.; Boreman, G. D.; Raschke, M. B. Optical dielectric function of silver. *Phys. Rev. B* **2015**, *91*, 235137.

(55) Olmon, R. L.; Slovick, B.; Johnson, T. W.; Shelton, D.; Oh, S.-H.; Boreman, G. D.; Raschke, M. B. Optical Dielectric Function of Gold. *Phys. Rev. B* **2012**, *86*, 235147.

(56) Puchkova, A.; Vietz, C.; Pibiri, E.; Wünsch, B.; Sanz Paz, M.; Acuna, G. P.; Tinnefeld, P. DNA Origami Nanoantennas with over 5000-fold Fluorescence Enhancement and Single-Molecule Detection at 25 μM. *Nano Lett.* **2015**, *15*, 8354–8359.

(57) Gopinath, A.; Thachuk, C.; Mitskovets, A.; Atwater, H. A.; Kirkpatrick, D.; Rothemund, P. W. K. Absolute and Arbitrary Orientation of Single-Molecule Shapes. *Science* **2021**, *371*, eabd6179.

(58) Adamczyk, A. K.; Huijben, T. A. P. M.; Sison, M.; Di Luca, A.; Chiarelli, G.; Vanni, S.; Brasselet, S.; Mortensen, K. I.; Stefani, F. D.; Pilo-Pais, M.; Acuna, G. P. DNA Self-Assembly of Single Molecules with Deterministic Position and Orientation. *ACS Nano* **2022**, *16*, 16924–16931.

(59) Carnegie, C.; Griffiths, J.; de Nijs, B.; Readman, C.; Chikkaraddy, R.; Deacon, W. M.; Zhang, Y.; Szabó, I.; Rosta, E.; Aizpurua, J.; Baumberg, J. J. Room-Temperature Optical Picocavities below 1 nm3 Accessing Single-Atom Geometries. *J. Phys. Chem. Lett.* **2018**, *9*, 7146–7151.